Article:

Jia, J, Wang, M and Faraj, Y (2014) Evaluation of EIT systems and algorithms for handling full void fraction range in two-phase flow measurement. Measurement Science and Technology, 26 (1). 015305. ISSN 0957-0233

https://doi.org/10.1088/0957-0233/26/1/015305

Evaluation of EIT Systems and Algorithms for Handling Full Void Fraction Range in Two-phase Flow Measurement

Jiabin Jia[b], Mi Wang[a] and Yousef Faraj[a]

[a] School of Chemical and Process Engineering, University of Leeds, Leeds, LS2 9JT, UK
[b] School of Engineering, University of Edinburgh, Edinburgh, EH9 3JL , UK
jiabin.jia@ed.ac.uk, m.wang@leeds.ac.uk, y.faraj@leeds.ac.uk

Abstract: In the aqueous-based two-phase flow, if the void fraction of dispersed phase exceeds 0.25, the conventional Electrical Impedance Tomography (EIT) produces a considerable error due to the linear approximation of Sensitivity Back-projection method, which limits the EIT's wider application in process industry. In this paper, an EIT sensing system which is able to handle full void fraction range in two-phase flow is reported. This EIT system employs a voltage source, conducts true mutual impedance measurement and reconstructs online image with the Modified Sensitivity Back-projection algorithm. The capability of Maxwell relationship to convey full void fraction is investigated. The limitation of linear sensitivity back-projection method is analysed. The modified sensitivity back-projection method is used to derive relative conductivity change in the evaluation. Series of static and dynamic experiments demonstrate the mean void fraction obtained by this EIT system has a good agreement with reference void fractions over the range from 0 to 1, which will significantly extend the applications of EIT in process measurement.

Keywords: Electrical Impedance Tomography, Two-phase flow measurement, Full void fraction and Voltage source EIT

1. INTRODUCTION

Gas-liquid two phase flow exists in many process industries. Electrical Impedance Tomography (EIT) is an imaging technique providing both cross-sectional image of gas distribution and mean gas void fraction of two phase flow. The gas void fraction in two phase flow was studied using different tomographic modalities. Shaikh applied a single source γ-ray Computed Tomography on the 0.0162 m diameter bubble column and the mean gas void fraction at ambient conditions was tested up to 0.32 [1]. The Wire-mesh Sensor (WMS) was used to characterise the radial gas void fraction profiles on the 0.067 m diameter and 6 m length vertical pipe [2]. The maximum gas volume fraction presented on the centre of the pipe was 0.92 when the superficial velocity of water and gas were 0.20 m/s and 3.32 m/s respectively. The mean gas void fraction was measured up to 0.70. In the previous study of using EIT for two phase flow measurement, the void fraction range managed by EIT was much narrower. For instance, the maximum oil volume fraction was 0.23 on Li's experiment [3]. The maximum gas void fraction in Jin's study was below 0.25 [4]. The gas void fraction reached 0.64 in Dong's study [5], but the void fraction was estimated based on the polynomial regression of measurement voltage values.

A comparison study between the Leeds FICA EIT system [6] and the Wire-mesh sensor (WMS) [7] was conducted to validate the accuracy of EIT measurement for air void fraction in air-water two phase upwards flows [8]. The image reconstruction algorithm used was Modified Sensitivity Back-Projection (MSBP). As shown in Figure 1, the air void fractions obtained from two tomographic systems had very good agreement when less than 0.25. However, compared with WMS, the EIT gradually underestimated the air void fraction when beyond 0.25. The error trend for air void fraction higher than 0.45 was not examined due to the limitations of the experimental flow loop, but a further underestimation was expected. Therefore, it is worthwhile to investigate this phenomenon and expand the capability of EIT to handle full void fraction range of dispersed phase from 0 to 1 in two phase flow.

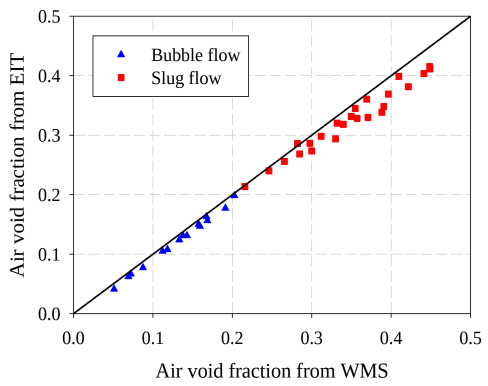

Figure 1. Comparison of overall air void fraction between EIT and WMS [7].

Electrical Impedance Tomography (EIT) was initially invented for medical imaging applications [9-10]. The alternating current source was applied to drive the electrodes, because the magnitude of current injected into to human body can be controlled within the safety limit. Later, the applications of EIT technique were utilized for industrial process measurement, but the majority of EIT systems still kept current as excitation source and sensed voltages as shown in Figure 2 (a). The EIT with current source has following disadvantages. When aqueous continuous phase is not very conductive, for example distilled water, response voltages on the sensing electrodes could exceed the maximum input range of the analogue to digital converter, particularly after the addition of non-conductive dispersed phase. The saturated voltage signal cannot reflect any change of two phase flow. When continuous phase is highly conductive like sea water, the equivalent mutual impedance is in the order of ohm, only using large current drive (hundreds mA) can increase the magnitude of response voltage on the electrodes for measurement. However, it is difficult to design a current source having more than 75mA output in the typical EIT frequency range 1kHz-1MHz. Moreover, the output of current source does not maintain constant while the load varies. In SPICE simulation of an EIT's current source [6], the load impedance is swept from 5Ω to 1255Ω and the output amplitude of the current source has 5.93% decrease, which brings in additional error for EIT measurement if this defect of current source is not taken into account. These limitations of current source restrict the performance and accuracy of EIT.

A recently developed EIT system [11] applies voltage to electrodes as excitation source. The output current of the voltage source and voltages across electrodes are monitored simultaneously to calculate mutual impedance (Z=V/I) in the voltage source EIT, which is the variable of the image reconstruction algorithm in section 3 rather than the voltage values in the current source EIT system. Figure 2 (a) and (b) illustrate two structures of EIT. The mechanism of the voltage source EIT overcomes the limit of current source associated with the conventional EIT systems.

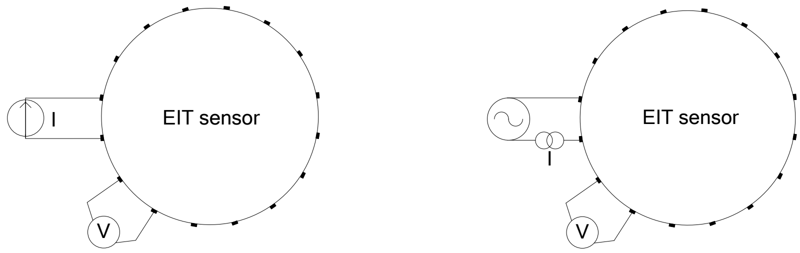

(a) Current source EIT (b) Voltage source EIT

Figure 2. Schematic of EIT measurement

2. CAPABILITY OF MAXWELL RELATIONSHIP FOR FULL VOID FRACTION

In EIT, by solving the inverse problem, the tomographic image showing the electrical conductivity contrast is reconstructed using N mutual impedance data acquired from all the impedance projections to visualise the distribution of dispersed phase. A conductivity image consists of M square pixels, which are 316 in authors' case. More information can be deduced from the conductivity image, for instance, the local and overall void fraction of the dispersed phase. Different correlations were proposed to convert electrical conductivity on each image pixel into the corresponding void fraction of dispersed phase [12].

The Maxwell relationship [13] formulated in equation (1) is mostly used to derive void fraction from conductivity.

$$\alpha = \frac{2\sigma_1 + \sigma_2 - 2\sigma_{\mathrm{mc}} - \dfrac{\sigma_{\mathrm{mc}}\sigma_2}{\sigma_1}}{\sigma_{\mathrm{mc}} - \dfrac{\sigma_2}{\sigma_1}\sigma_{\mathrm{mc}} + 2(\sigma_1 - \sigma_2)} \tag{1}$$

where σ_1 is the conductivity of aqueous continuous phase (water), σ_2 is the conductivity of dispersed phase (air or oil), σ_{mc} is the mixture conductivity obtained from EIT and α is local void fraction. α, σ_1, σ_2 and σ_{mc} are the vectors with M elements (M=316 in authors' case) and each element represents the value in the local area. If dispersed phase is non-conductive, σ_2 is assumed to be zero and equation (1) is simplified as:

$$\alpha = \frac{2\sigma_1 - 2\sigma_{\mathrm{mc}}}{\sigma_{\mathrm{mc}} + 2\sigma_1} \tag{2}$$

Rearrange equation (2), the conductivity ratio $\sigma_{\mathrm{mc}}/\sigma_1$ becomes the only variable in equation (3) to determine the void fraction α.

$$\alpha = \frac{2 - 2\dfrac{\sigma_{\mathrm{mc}}}{\sigma_1}}{2 + \dfrac{\sigma_{\mathrm{mc}}}{\sigma_1}} \tag{3}$$

Equation (3) describes the correlation between two vectors. Each individual element of $\sigma_{\mathrm{mc}}/\sigma_1$ and α will satisfy the equation too. In air-water or oil-water two phase flows, the mixture conductivity σ_{mc} must be in the range of $0 \leq \sigma_{\mathrm{mc}} \leq \sigma_1$. Then, the conductivity ratio $\sigma_{\mathrm{mc}}/\sigma_1$ is $0 \leq \sigma_{\mathrm{mc}}/\sigma_1 \leq 1$. On one extreme condition, if the flow pipeline is full of non-conductive dispersed phase, like air or oil, the mixture conductivity σ_{mc} becomes 0 and the conductivity ratio $\sigma_{\mathrm{mc}}/\sigma_1$ equals to 0. Therefore, α in equation (3) is 1. On another extreme condition, if the flow pipeline is full of aqueous continuous phase, like water, the mixture conductivity σ_{mc} is identical with σ_1, and the conductivity ratio $\sigma_{\mathrm{mc}}/\sigma_1$ becomes 1 and α in equation (3) is 0, which means no dispersed phase presents in the mixture at all. For simplicity, Figure 3 graphically illustrates the correlation between one element of $\sigma_{\mathrm{mc}}/\sigma_1$ and the corresponding α. Although $\sigma_{\mathrm{mc}}/\sigma_1$ and α do not follow linear relationship with respect to equation (3), the void fraction obtained from equation (3) falls in the range of 0~1, provided that the conductivity ratio $\sigma_{\mathrm{mc}}/\sigma_1$ is known. Two algorithms of calculating $\sigma_{\mathrm{mc}}/\sigma_1$ will be compared in next section.

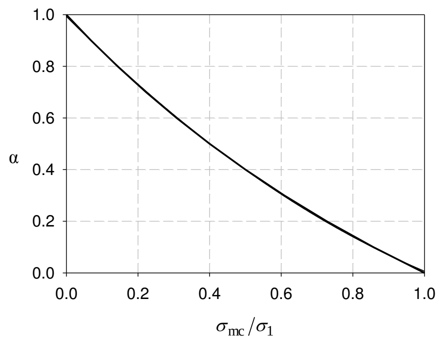

Figure 3. Relationship between the conductivity ratio σ_{mc}/σ_1 and void fraction α

3. IMAGE RECONSTRUCTION ALGORITHM

The process of image reconstruction in EIT is to determine the unknown electrical conductivity based on the known voltage on the electrodes or mutual impedance in our case. In fact, this is a nonlinear process in electrical tomography; moreover, the N number of the known mutual impedance is much less than the M number of unknown conductivity. These challenges make finding the precise unknown electrical conductivity very difficult. There are many image reconstruction algorithms were developed for EIT [14]. They are separated into two categories, qualitative non-iterative algorithms and quantitative iterative algorithms. Non-iterative algorithms only involve the multiplication between a matrix and a vector. Although the images reconstructed from these algorithms are not sharp and clear, their computational speed is so fast that only non-iterative algorithm can be implemented in EIT to conduct on-line measurement and control for multiphase flow. Iterative algorithms can deliver relatively better images but in the cost of longer computational time. These algorithms are suitable for the applications requiring higher quality to the off-line images for instance medical imaging. Since the targeted application in this paper is dynamic multiphase flow measurement, only non-iterative algorithms are discussed.

Due to the addition of dispersed phase, the change of mutual impedance ΔZ and the change of conductivity $\Delta\sigma$ in the medium are respectively defined as

$$\Delta Z = Z_{mc} - Z_1 \tag{4}$$

$$\Delta\sigma = \sigma_{mc} - \sigma_1 \tag{5}$$

where Z_1 is the baseline mutual impedance measured from EIT sensor containing only single continuous phase with conductivity σ_1. Z_{mc} is mutual impedance after two phase mixture presents and conductivity is altered to σ_{mc}.

Computing the change of mutual impedance ΔZ from the known conductivity change $\Delta\sigma$ is a forward process and described as

$$\Delta Z = F(\Delta\sigma) \tag{6}$$

where F is a forward operator and can be solved by the finite element methods.

An alternative approach to solve equation (6) is to use Taylor series in equation (7)

$$\Delta Z = \frac{\partial F}{\partial \sigma}(\Delta\sigma) + O((\Delta\sigma)^2) \tag{7}$$

Based on the condition of $\Delta\sigma << \sigma_1$, high order terms $O((\Delta\sigma)^2)$ is omitted and equation (7) is linearized into equation (8). If the condition of $\Delta\sigma << \sigma_1$ cannot be satisfied, large numerical error will occur.

$$\Delta Z = -S' \cdot \Delta\sigma \tag{8}$$

where $S' = \partial F(\sigma_1)/\partial\sigma_1$ is defined as sensitivity matrix and σ_1 is the baseline conductivity. The minus sign of equation (8) indicates conductivity and mutual impedance have opposite change direction. The normalised form of equation (7) is expressed as:

$$\frac{\Delta Z}{Z_1} = -S \cdot \frac{\Delta\sigma}{\sigma_1} \tag{9}$$

Where S is the normalised sensitivity matrix and formulated as equation (10), i is the location of excitation-measurement projection, k is the pixel number and M is the total number of image pixels.

$$S = \frac{S'_{i,j}}{\sum_{k=1}^{M} S'_{i,k}} \tag{10}$$

To find the relative conductivity changes $\Delta\sigma/\sigma_1$ from the relative mutual impedance changes $\Delta Z/Z_1$ is the inverse process of equation (9), which still remains a challenge to find the exact inverse matrix of S in EIT imaging. Kotre [15] developed the Sensitivity Back-Projection (SBP) algorithm based on the Linear Back-Projection (LBP) principle, where inverse S^{-1} is approximated to its transpose matrix S^T as shown in equation (11), because S is not a square matrix. This approximation gives the best fit from the least square point of view, but it could not be the best operator for all the applications [16].

$$\frac{\Delta\sigma}{\sigma_1} = -S^{-1} \cdot \frac{\Delta Z}{Z_1} \approx -S^T \cdot \frac{\Delta Z}{Z_1} \tag{11}$$

Substitute equation (4) and (5) into equation (11), the first method of calculating σ_{mc}/σ_1 is illustrated in equation (12).

$$\frac{\sigma_{mc}}{\sigma_1} \approx 1 - S^T \cdot \frac{Z_{mc} - Z_1}{Z_1} \tag{12}$$

In equation (13), the modified Sensitivity Back-Projection (MSBP) based on the nonlinear approximation [17] was proposed as an alternative approach to gain σ_{mc}/σ_1.

$$\frac{\sigma_{mc}}{\sigma_1} \approx \frac{1}{S^T \cdot \frac{Z_{mc}}{Z_1}} \tag{13}$$

Substitute equation (12) and (13) into equation (3) individually, the ultimate correlations between void fraction α and mutual impedance ratio Z_{mc}/Z_1 are expressed in equation (14) and (15).

$$\alpha \approx \frac{2S^T \cdot \frac{Z_{mc}}{Z_1} - 2S^T}{3 - S^T \cdot \frac{Z_{mc}}{Z_1} + S^T} \tag{14}$$

$$\alpha \approx \frac{S^T \cdot \frac{Z_{mc}}{Z_1} - 2}{2S^T \cdot \frac{Z_{mc}}{Z_1} + 1} \tag{15}$$

α in equation (14) and (15) contains M elements representing the void fraction of dispersed phase in local image pixel area. The overall cross-sectional void fraction A is the average of M element in α.

$$A = \frac{\sum_{i=1}^{M} \alpha_i}{M} \tag{16}$$

In order to visualise the correlation between mean void fraction A and mutual impedance ratio Z_{mc}/Z_1 in an ideal and simply perspective, it is assumed that the vector Z_{mc}/Z_1 has N elements with the same value. Two correlations are plotted in Figure 4. The logarithm scale is applied for the x-axis Z_{mc}/Z_1 to demonstrate a wider Z_{mc}/Z_1 range. The red dashed curve in Figure 5 shows that in MSBP algorithm, the mean void fraction does not exceed the range of 0~1 with respect to the variation of Z_{mc}/Z_1 from 1 to 1000, despite the correlation is not in linear relationship. On the contrary, the blue solid curve indicates the correlation of SBP algorithm is not a monotonic function and the limit of the SBP correlation exists in the Z_{mc}/Z_1

range of 3.95~4.00. Figure 5 suggests the SBP algorithm only can present meaningful and valid results when Z_{mc}/Z_1 is less than 2. Other values of Z_{mc}/Z_1 result in the mean void fraction beyond the range of 0~1.

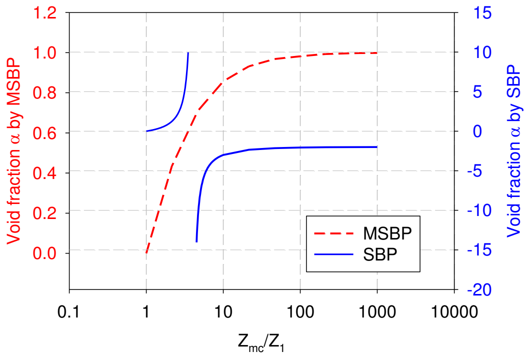

Figure 4. Correlation of mutual impedance ratio Z_{mc}/Z_1 and mean void fraction A

To compare two correlations only in the valid range of SBP algorithm, Figure 4 is re-plotted into Figure 5 only when the conductivity ratio Z_{mc}/Z_1 is from 1 to 2.2. Both correlations output 0 void fraction when Z_{mc}/Z_1 equals to 1, however, the divergence of SBP and MSBP is dramatically intensified once Z_{mc}/Z_1 is larger than 1.6. It is concluded that the MSBP algorithm is a better correlation than the SBP algorithm. In the next section, only MSBP algorithm is applied for the computation of void fraction.

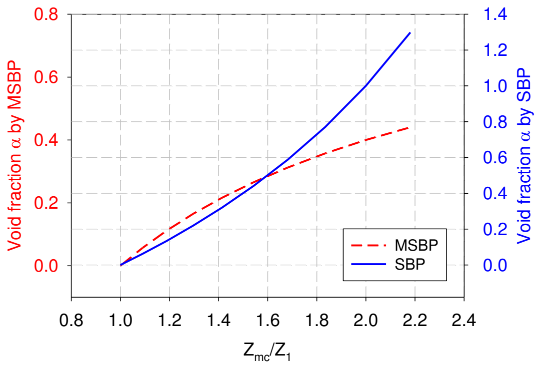

Figure 5. Valid Z_{mc}/Z_1 range of SBP in Figure 4

4. EXPERIMENTS

4.1 Dynamic Experiment: Air-Water Two Phase Flow

The experiment was conducted out in a Perspex flow loop with 0.058 m inner diameter of and 3.0 m vertical section. The detailed schematic of the experimental flow loop is referred in literature [7]. The mean air void fractions obtained from the voltage source EIT system [11] and Wire-mesh sensor (WMS) are compared in Table 1. At the flow conditions with air void fraction range less than 0.30; the void fraction delivered by EIT is close to that of WMS.

Table 1. Air void fraction measured by WMS and EIT

Flow condition		Air void fraction	
Water flow rate	Air flow rate(m^3/s)	WMS	EIT
$2.04x10^{-3}$	$8.33x10^{-5}$	0.04345	0.04432
$9.32x10^{-4}$	$8.33x10^{-5}$	0.05978	0.06828
$2.04x10^{-3}$	$8.33x10^{-4}$	0.22892	0.23263
$9.32x10^{-4}$	$8.33x10^{-4}$	0.29673	0.31884

4.2 Static EIT Vessel Experiment: Packed Particles

Due to the capability of the existing laboratory flow loop, it is difficult to create a flow regime with air void fraction larger than 0.5. In order to create two phase mixture having larger void fractions, a number of static setups with the packed particles were used. A 50.8mm diameter static EIT vessel was filled up with 305.0mL tap water for the reference baseline taken by EIT. Later, non-conductive yellow spherical particles with 6.00mm diameter were gradually poured into the vessel. At the same time, water was carefully removed and collected from the vessel, until the mixture reaches the same water level as the reference setup, to keep the total volume of mixture the same as 305.0mL. The volume of water repelled by particle was 175.0mL. As shown in Figure 6(a), particles were randomly packed and the mixture was regarded as homogenous. The true void fraction of particles was calculated as 0.5738 (175.0mL/305.0mL). The measured void fraction of EIT using equation (15) was 0.5922. Since particles are homogenous packed, the 2D cross-sectional void fraction measured by EIT can represent the real 3D void fraction estimated by the volume ratio of particles and water.

To further increase the void fraction, the pervious experiment procedure was repeated. The only difference was the second type of non-conductive blue particles with 0.72mm diameter were carefully poured into the vessel as well when the 6.00mm particles were poured into the vessel as shown in Figure 6 (b). These fine purple particles filled in the space between the larger yellow particles, so a larger void fraction was expected. At this time 222.5mL tap water was repelled. The actual void fraction of particles was calculated as 0.7295 (222.5mL/305.0mL). Whereas, the void fraction measured by EIT was 0.7216.

(a) (b)

Figure 6. Spherical non-conductive particle randomly packed in the static EIT vessel (a) 6.00mm (b) 6.00mm and 0.72mm.

The radial void fraction profiles of two static experiments are demonstrated in Figure 7. Both black and blue curves exhibit the uniform particle distribution and void fraction cross the centre to the boundary of the tube. Because the particles are scattered into the tube manually, it might cause the minor fluctuation on the void fraction profiles.

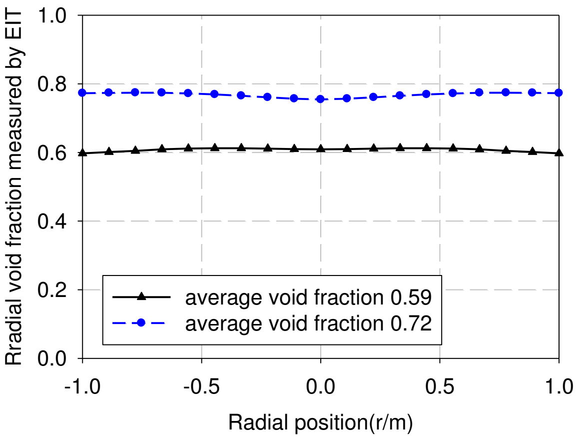

Figure 7. Radial void fraction profile

4.3 Static EIT Vessel Experiment: Full and Empty

Two extreme conditions, void fraction 0 and 1, is tested in this experiment. When the vessel was full of tap water in Figure 8(a), the void fraction shown from the EIT was 0.0006. Later, tap water was drained out completely in Figure 8(b). The EIT system indicates void fraction 0.9878 for this setup.

(a) (b)

Figure 8. Full (a) and empty (b) EIT vessel.

The void fractions of dispersed phase from all pervious experiments are plotted against reference void fractions in Figure 9. The first and last black points are referred to the full and empty EIT sensor respectively. Four blue points are from air-water flow measurement and referred to the Wire-mesh sensor in the experiment 4.1. Two red points are referred to the volumetric ratio between particles and total mixture in the experiments 4.2. A strong linear relationship between the measured void fraction by EIT and reference void fraction presented in Figure 11.

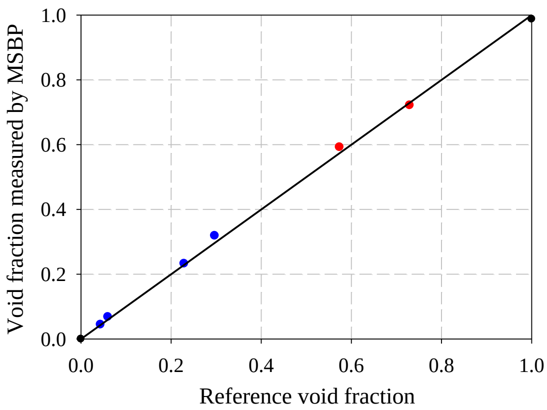

Figure 9. Void fractions presented by EIT from different experiments vs. reference void fraction.

4.5 Dynamic Experiment: Bubble column

A qualitative dynamic air-water flow experiment was carried out on a 50.8mm water column mounted with EIT sensors. The column was empty up to frame number 172. The EIT system showed 0.9918 air void fraction. Tap water was perfused from the bottom of the column. From frame number 215 to 428, there was full water in the column. The air void fraction dropped down to 0.0006. Then, air was freely blown from the bottom into the water column until frame 922. The variation of the air void fraction was recorded by the EIT system. From frame 923 to 1101, there was no air injection and the column remained water only condition. Finally, water was drained out and the column was empty from frame 1129. Figure 10 shows the dynamic change of the air void fraction during whole process. Future work will involve verifying the air void fraction through entire void fraction range using other sensing modalities, particularly for the period of frame number 428 to 922. The author infers that the measurement accuracy of the voltage source EIT system and MSBP algorithm depends on the flow regime. Homogeneous and quasi-homogenous flow regime will be the ideal application scenario. If EIT electrodes lose electric contact with the continuous phase, for instance horizontal stratified flow, the measurement error still remains a challenge.

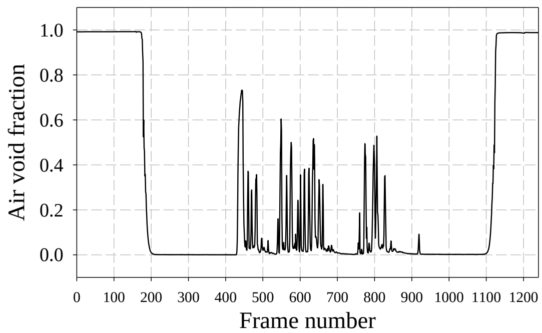

Figure 10. Dynamic air void fraction recorded by EIT.

5. CONCLUSIONS

The conventional Electrical Impedance Tomography (EIT) with current source tends to underestimate the void fraction of dispersed phase in two phase flow measurement when it is larger than 0.25. The EIT system with the voltage source simultaneously measures voltage and current then calculates the mutual impedance of two phase flow, which overcomes the limit of the conventional current source EIT. The Maxwell relationship has the capability to represent the correlation between relative conductivity change and void fraction in the full 0 to 1 range. The Sensitivity Back-Projection (SBP) algorithm works only when the conductivity has minor change which restricts the application of EIT to wider flow regimes. The

Modified Sensitivity Back-Projection (MSBP) algorithm is a better conversion from impedance to conductivity. The performance of the voltage source EIT system over a full void fraction range is evaluated. The experimental results demonstrate the full void fraction range of two phase flow can be managed by the EIT system with voltage source.

REFERENCES

1. A. Shaikh, M. Al-Dahhan, “Characterization of the hydrodynamic flow regime in bubble columns via computed tomography”, Flow Measurement and Instrumentation, Volume 16, Issues 2–3, April–June 2005, Pages 91-98
2. L. Szalinski, L.A. Abdulkareem, M.J. Da Silva, S. Thiele, M. Beyer, D. Lucas, V. Hernandez Perez, U. Hampel, B.J. Azzopardi, Comparative study of gas–oil and gas–water two-phase flow in a vertical pipe, Chemical Engineering Science, Volume 65, Issue 12, 15 June 2010, Pages 3836-3848
3. H. Li, M. Wang, Y-X. Wu and G. Lucas, “Volume flow rate measurement in vertical oil-in-water pipe flow using *electrical impedance tomography and local”, 11*th Int. Conf. on Multiphase Flow in Industrial Plants, Palermo, Italy, 200.8
4. H. Jin, Y. Lian, S. Yang, G. He and Z. Guo, “The parameters measurement of air–water two phase flow using the electrical resistance tomography (ERT) technique in a bubble column”, Flow Measurement and Instrumentation, Volume 31, June 2013, Pages 55-60.
5. F. Dong, Z.X. Jiang, X.T. Qiao, L.A. Xu, “Application of electrical resistance tomography to two-phase pipe flow parameters measurement”, Flow Measurement and Instrumentation, Volume 14, Issues 4–5, August–October 2003, Pages. 183-192.
6. M. Wang, Y. Ma, N. Holliday, Y. Dai, R. A. Williams, and G. Lucas, “A High-performance EIT System”, IEEE Sensors Journal 5(2): 2005, Pages. 289-299.
7. C. Olerni, J. Jia and M. Wang, “Measurement of Air Distribution and Void Fraction of an Upward Air-water Flow Using Electrical Resistance Tomography and Wire-mesh Sensor”, Measurement Science and Technology Volume 24, No. 3, 2013.
8. H. -M. Prasser, A. Böttger and J. Zschau, “A New Electrode-mesh Tomograph for Gas–liquid Flows”, Flow Measurement and Instrumentation, Volume 9, Issue 2, 1998, Pages 111-119.
9. Henderson, R.P.; Webster, J.G. (1978). "An Impedance Camera for Spatially Specific Measurements of the Thorax". IEEE Trans. Biomed. Eng. 25 (3): 250–254.
10. Barber, D.C.; Brown, B.H. (1984). "Applied Potential Tomography". J. Phys. E:Sci. Instruments 17 (9): 723–733.A.
11. J. Jia, M. Wang, H. I. Schlaberg and H. Li, “A Novel Tomographic Sensing System for High Electrically Conductive Multiphase Flow Measurement”, Flow Measurement & Instrumentation. 21, 2010, Pages. 184-190.
12. V.S. Shirhatti, “Characterisation and Visualisation of Particulate Solid-liquid Mixing Using Electrical Resistance Tomography”, Ph.D. Thesis, University of Leeds, 2007.

13. J. C. A. Maxwell, “Treatise on Electricity and Magnetism”, Unabridged Third edition, Volume 1, Dover Publications Inc. New York, 1954.

14. W. R. B. Lionheart, “EIT reconstruction algorithms: pitfalls, challenges and recent developments”, Physiol Meas. Volume 25, 2004, pp. 125-142.

15. C. J. Kotre, “EIT Image Reconstruction Using Sensitivity Weighted Filtered Back-projection”, Physiol Meas. Volume 15, 1994, pp. 125–136.

16. T. Dyakowski, F. C. J. Laurent, A. J. Jaworski, “Applications of electrical tomography for gas-solids and liquid-solids flows -a review” Volume 112, Issue 3, 2000, Pages 174-192

17. M. Wang, “Inverse Solutions for Electrical Impedance Tomography Based on Conjugate Gradients Methods”, Measurement Science and Technology Vol. 13, Issue 1, 2001, pp. 101-117.